Journal of Structural Geology 30 (2008) 827–838

Contents lists available at ScienceDirect

Journal of Structural Geology

journal homepage: www.elsevier.com/locate/jsg

Total bulk strain in flattened parallel folds

J. Aller [a,*], N.C. Bobillo-Ares [b], F. Bastida [a], R.J. Lisle [c]

[a] Departamento de Geología, Universidad de Oviedo, Jesús Arias de Velasco s/n, 33005 Oviedo, Asturias, Spain
[b] Departamento de Matemáticas, Universidad de Oviedo, 33007 Oviedo, Spain
[c] School of Earth and Ocean Sciences, Cardiff University, Cardiff CF10 3YE, UK

ARTICLE INFO

Article history:
Received 27 August 2007
Received in revised form 5 March 2008
Accepted 27 March 2008
Available online 8 April 2008

Keywords:
Fold flattening
Buckling
Strain
Mathematical modelling

ABSTRACT

A new simple method is proposed to analyse the total bulk shortening in flattened parallel folds. Application of the method requires determining first the amount of flattening using any of the available techniques or by using a new method proposed in this paper. Then, some shape information must be obtained from the fold, such as the interlimb angle or the aspect ratio, as well as the eccentricity of the conic section that gives the best fit to the midline of the folded layer. The latter parameter can be obtained using the program "Fold Profiler". Finally, the flattening and the shape data are used to obtain the total bulk shortening of the folded layer. A computer code is provided that performs these calculations. The method does not consider the initial layer shortening prior to buckling and therefore gives an estimate of the minimum bulk shortening associated with the fold. The strain data obtained with this method are not point values from selected locations inside the folded structure, but an overall evaluation of its bulk strain that can be advantageously used in the regional interpretation. The analysis is two-dimensional and only considers deformation in the fold profile plane. The study is completed with an example of the application of the method to natural folds.

1. Introduction

The analysis of strain in rocks and its variation within orogenic belts is an important task of structural geology. Unfortunately, good strain markers are not common, especially in metamorphic zones, and available methods to achieve these goals are often laborious. Moreover, the accuracy of the results obtained is uncertain in some cases. As a result of all these problems, the distribution of strain is not well known at present in many orogens. Analysis of strain using folds is an alternative to the traditional methods, since fold structures are common and their morphology and cleavage patterns can be used advantageously to shed light on the strain distribution in the folded layers. In particular, the analysis of the geometry of flattened parallel folds (Ramsay, 1962, 1967; Mukhopadhyay, 1965) affords valuable and simple tools for the estimation of the strain associated with folding (Ramsay, 1967; Hudeleston, 1973; Lisle, 1992, 1997; Hudleston and Lan, 1993; Bastida et al., 2003, 2005; Shah and Srivastava, 2006; Srivastava and Shah, 2006; among others).

Flattened parallel folds are formed from parallel folds (class 1B) by the superposition of an irrotational homogeneous strain involving a shortening perpendicular to the axial surface. The previous parallel folds develop as a result of buckling by kinematical mechanisms such as flexural flow or tangential longitudinal strain. The folds resulting from this superimposition have class 1C shapes (Ramsay, 1967, pp. 411–415). Determining the total bulk shortening of these folds is possible by finding first the bulk shortening associated with flattening and then the bulk shortening associated with buckling.

Several methods have been developed to determine the bulk strain associated with flattening. Ramsay (1962, 1967) and Mukhopadhyay (1965) found a functional relation between the orthogonal thickness of the folded layer, the ratio $r_f = \sqrt{\lambda_2/\lambda_1}$ of the axial lengths of the flattening strain ellipse and the dip of the layer. Another method to measure the amount of flattening and to classify folds was developed by Lisle (1997), who used for this purpose the polar plot of the coordinates of the inverse orthogonal thickness ($1/t_\alpha$ or $1/t'_\alpha$) vs. the dip α. Srivastava and Shah (2006) proposed a method to obtain the amount of flattening by destraining the flattened parallel fold with the help of the commonly available drafting software. Other procedures, based on the Wellman method and the Mohr circle, were developed by Shah and Srivastava (2006).

Although several methods exist for quantifying the amount of flattening involved in flattened parallel folds, there are no analytical or graphical methods to directly obtain the total bulk shortening involved in this type of folds. Furthermore, ideally such methods

* Corresponding author. Tel.: +34 98 510 3119; fax: +34 98 510 3103.
E-mail address: aller@geol.uniovi.es (J. Aller).

0191-8141/$ – see front matter © 2008 Elsevier Ltd. All rights reserved.
doi:10.1016/j.jsg.2008.03.005

should take into account the bulk shortening involved at the buckling stage. The aim of this paper is to develop a new simple method that can be used to obtain bulk strain estimates from flattened parallel folds. The method can be applied to a fold even if we only know its limb–hinge thickness ratio and its general shape, and it gives an estimation of the minimum bulk shortening associated with the fold. This approach can be helpful for fast strain estimations of the overall strain in cases where other methods are difficult to apply. On the other hand, strain data obtained with this method are not point values from selected locations inside the structure, but a general evaluation of the bulk strain of the fold that can be advantageously used in the regional interpretation. The analysis is two-dimensional and only considers deformation in the fold profile plane. The study is completed with an example of application of the method to natural folds.

2. Basis of the method

The proposed method allows the total bulk shortening associated with development of flattened parallel folds to be determined. It involves assuming a two-stage evolution of the fold: (i) formation of a parallel or near parallel fold by buckling mechanisms such as parallel tangential longitudinal strain (Bobillo-Ares et al., 2006), equiarea tangential longitudinal strain (Ramsay, 1967, pp. 397–403; Bobillo-Ares et al., 2000, 2006), flexural flow, or a combination of these, and (ii) superposition of an irrotational homogeneous strain with maximum shortening perpendicular to the axial trace of the buckling fold, producing a class 1C fold (Ramsay, 1967, pp. 411–415). The analysis is focussed on symmetrical folds, but it can be extended in some cases to asymmetrical folds formed by superposition of a more general homogeneous strain on buckling folds.

The analysis requires considering three successive configurations of the fold (Fig. 1): I, initial configuration; II, configuration after buckling; and III, configuration after flattening. Each stage is represented by the midline of the layer. It is assumed that the length of this line l_0 does not change during buckling (transformation from I to II). The coordinates of a point p on the midline in the configuration after buckling and those of its image p' after flattening are related by

$$x' = \sqrt{\lambda_2}x, \quad y' = \sqrt{\lambda_1}y, \tag{1}$$

where $\sqrt{\lambda_1}$ and $\sqrt{\lambda_2}$ are the principal stretches of the flattening. Hence, functions $g(x)$ and $f(x')$, which represent the midline in the configurations II and III, respectively, are related according to

$$g(x) = \frac{1}{\sqrt{\lambda_1}} f\left(\sqrt{\lambda_2}x\right). \tag{2}$$

The bulk shortenings involved in the evolution of the fold are as follows (Fig. 1).

- Buckling bulk shortening:

$$\varepsilon = \frac{l_0 - 2x_0}{l_0}. \tag{3}$$

- Flattening bulk shortening:

$$\varepsilon' = \frac{2x_0 - 2x'_0}{2x_0}. \tag{4}$$

- Total bulk shortening:

$$\varepsilon_T = \frac{l_0 - 2x'_0}{l_0}. \tag{5}$$

These shortenings are related by the following equation:

$$\varepsilon_T = \varepsilon + \varepsilon' - \varepsilon\varepsilon'. \tag{6}$$

Taking into account the first of the Eq. (1), the definitions (3), (4) and (5) can be written in terms of x'_0, which can be measured in the field, and of l_0:

$$\varepsilon = 1 - \frac{2x'_0}{\sqrt{\lambda_2}l_0}, \tag{7}$$

$$\varepsilon' = 1 - \sqrt{\lambda_2}, \tag{8}$$

$$\varepsilon_T = 1 - \frac{2x'_0}{l_0}. \tag{9}$$

In order to obtain l_0 in terms of field data, the equation for the length of a curve must be used. Then

$$l_0 = 2\int_0^{x_0} \sqrt{1 + g'(x)^2}\,dx, \tag{10}$$

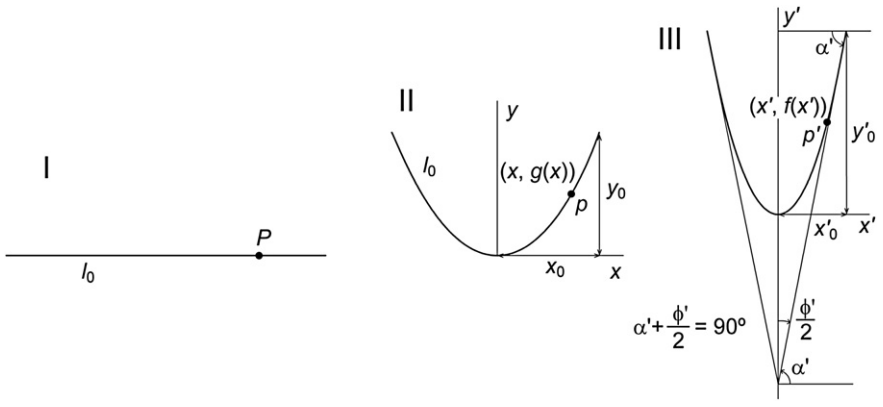

Fig. 1. Successive configurations of the folded layer midline. (I) Initial stage showing a general point P. (II) Configuration after buckling, showing the transformed general point $p\,(x, g(x))$. The midline length is preserved at this stage. (III) Configuration after flattening showing the transformed point $p\,(x', f(x'))$. See text for further explanation.

$g'(x)$ being the derivative of $g(x)$. Using Eq. (2) and simple variable change ($x' = \sqrt{\lambda_2}x$), we can write l_0 in terms of the midline $f(x')$ of configuration III:

$$l_0 = \frac{2}{\sqrt{\lambda_2}}\int_0^{x'_0}\sqrt{1+\frac{\lambda_2}{\lambda_1}f'(x')^2}\,dx', \tag{11}$$

$f'(x')$ being the derivative of $f(x')$.

A good fit to the midline of a natural fold can be obtained by a part of an adequately selected conic section. The general equations of this family of curves, in terms of the eccentricity e and a scale parameter a, are given by (Aller et al., 2004)

$$f(x')\begin{cases} a\dfrac{1-\sqrt{1-(1-e^2)\left(\frac{x'}{a}\right)^2}}{1-e^2} & 0 \le e \neq 1. \\ \dfrac{x'}{2a} & e = 1. \end{cases} \tag{12}$$

The parameter a can be obtained from the fold aspect ratio $h = y'_0/x'_0$ (Fig. 1) by the equation (Aller et al., 2004):

$$a = x'_0\frac{1+h^2(1-e^2)}{2h}. \tag{13}$$

The derivative function of $f(x')$ is

$$f'(x') = \frac{x'/a}{\sqrt{1-(1-e^2)\left(\frac{x'}{a}\right)^2}}. \tag{14}$$

Flattening maps ellipses to ellipses, parabolas to parabolas and hyperbolas to hyperbolas, that is, the type of conic section that represents the midline of the buckled layer does not change with flattening. Nevertheless, with the increase of the flattening amount, the aspect ratio increases and the eccentricity changes, except in the parabola, and tends progressively towards unity; that is, with the increase of flattening and aspect ratio, the shape of the fold profiles converges towards the parabola.

By introducing Eq. (14) into Eq. (11) we can obtain expressions for l_0 for the different values of the eccentricity e. Using the notation

$$V = \sqrt{|e^2-1|}\frac{x'_0}{a},\quad m = 1+\frac{\lambda_2}{\lambda_2(e^2-1)},\quad K = \frac{2a}{\sqrt{|e^2-1|}\sqrt{\lambda_2}},$$

$$b = \sqrt{\frac{\lambda_2}{\lambda_1}}\frac{x'_0}{a}, \tag{15}$$

we have

$$l_0 = K\int_0^V\sqrt{\frac{1-mv^2}{1-v^2}}\,dv \quad \text{for } 0 \le e < 1 \text{ (ellipses)}, \tag{16}$$

$$l_0 = K\int_0^V\sqrt{\frac{1+mv^2}{1+v^2}}\,dv \quad \text{for } e > 1 \text{ (hyperbolas)}. \tag{17}$$

The two integrals can be written in terms of elliptic functions of second kind (Abramowitz and Stegun, 1964). However, the value of these integrals can be obtained directly using MATHEMATICA™ or other mathematical software packages.

For the parabola ($e = 1$), the integral (11) can be written in terms of elementary functions.

$$l_0 = \frac{a\sqrt{\lambda_1}}{\lambda_2}\left(b\sqrt{1+b^2}+\operatorname{Arcsinh} b\right). \tag{18}$$

Some parameters that can be easily measured in the field or obtained from fold photographs and that can be used in the calculations are

- Maximum limb dip: α'.
- Interlimb angle: $\phi' = \pi - 2\alpha'$.
- Thickness ratio:
  $t = t'_{\alpha'}$(orthogonal thickness for the maximum limb dip)/(orthogonal thickness in the hinge(dip = 0)) $= (t_{\alpha'}/t_0)$.

The ratio r_f of the axes of the flattening ellipse in terms of $t'_{\alpha'}$ and α' (or ϕ') can be determined from the equation obtained by Ramsay (1967, p. 412, Eqs. (7)–(33)) for flattened parallel folds:

$$r_f = \sqrt{\frac{\lambda_2}{\lambda_1}} = \frac{\sqrt{t-\cos^2\alpha'}}{\sin\alpha'} = \frac{\sqrt{t-\sin^2\frac{\phi'}{2}}}{\cos\frac{\phi'}{2}}. \tag{19}$$

By introducing the area ratio (J = (area in the configuration III)/(area in the configuration II) $= \sqrt{\lambda_1\lambda_2}$) in Eq. (19) we can obtain λ_1 and λ_2:

$$\lambda_1 = J\frac{\sin\alpha'}{\sqrt{t-\cos^2\alpha'}}, \tag{20}$$

$$\lambda_2 = J\frac{\sqrt{t-\cos^2\alpha'}}{\sin\alpha'}. \tag{21}$$

Values of the area change $(J-1)$ are difficult to obtain in rocks and it can be considered close to unity for flattening in competent rocks. This unit value is assumed in the text below.

The scale parameter a can be determined from the interlimb angle ϕ' using the equation that gives the maximum slope of the limb midline ($\tan\alpha'$). For that it is necessary to determine the value of the derivative (14) in $x' = x'_0$:

$$\tan\alpha' = \frac{1}{\tan\frac{\phi'}{2}} = \frac{x'_0/a}{\sqrt{1-(1-e^2)(x'_0/a)^2}}. \tag{22}$$

From this equation the value of a is given by

$$a = x'_0\sqrt{\tan^2\frac{\phi'}{2}+(1-e^2)}. \tag{23}$$

3. Flattening and associated bulk shortening

The ratio r_f can be obtained by classifying the folded layer by Ramsay's (1967, pp. 359–372) method and comparing the plot of orthogonal thickness (t'_α) against dip with those corresponding to flattened parallel folds (Ramsay, 1967, p. 413, Figs. 7–79). Other different methods to obtain r_f have been proposed by Lisle (1997), Bobillo-Ares et al. (2004) and Srivastava and Shah (2006).

A simple evaluation of the r_f value can also be obtained by calculating parameters s_1 and s_2 for the fold analysed (Bastida et al., 2005). These parameters are defined from a curve of $t'_\alpha 2$ vs. $\sin^2\alpha$ for a fold limb, using two points, A and B, on this curve (Fig. 2). A is the point on the curve where the abscissa equals $(\sin^2\alpha_m)/2$, and B is the final point of the curve with abscissa $\sin^2\alpha_m$ (α_m is the maximum dip of the folded layer). After drawing the line segments, OA and AB, we define s_1 and s_2 as

$$s_1 = \tan\beta_1 = \frac{2\left(1-t'^2_1\right)}{\sin^2\alpha_m} \tag{24}$$

$$s_2 = \tan\beta_2 = \frac{2\left(t'^2_1-t'^2_2\right)}{\sin^2\alpha_m} \tag{25}$$

On an s_1–s_2 diagram, perfect flattened folds plot along the line $s_1 = s_2$. It is easy to show in this case that $s_1 = s_2 = 1 - r_f^2$, which

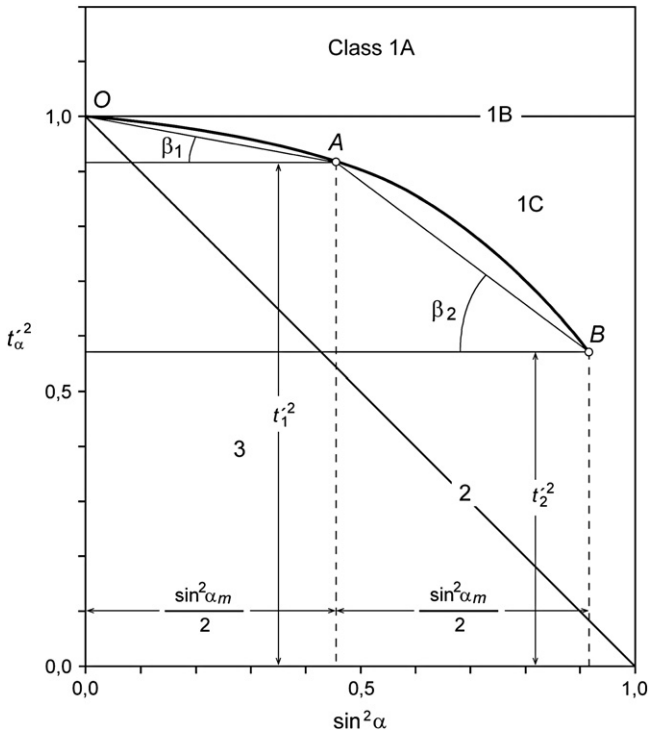

Fig. 2. Diagram of $t'_\alpha 2$ against $\sin^2\alpha$, and definition of angles β_1 and β_2, and t'_1 and t'_2 from a curve representative of a fold (after Bastida et al., 2005).

facilitates determining r_f from parameters s_1 and s_2. Some values of r_f have been plotted on the straight line $s_1 = s_2$ in Fig. 3. Points outside this line correspond to folds that diverge from the shape of a perfect flattened parallel fold, and the distance to this line gives an evaluation of the deviation. If the departure is not large, the arithmetic mean value of s_1 and s_2 can be used as an approximation to the r_f value of the analysed limb. The use of s_1 and s_2 allows the range of flattening undergone by a set of folds to be visualized in a single s_1–s_2 diagram.

The thickness ratio t is an interesting parameter which is closely related to the flattening of folds, since for a specific maximum dip α'_{max}, a single value of r_f corresponds to each thickness ratio t. This r_f value is given by Eq. (19). However, this method only gives a rough estimate, since it involves the assumption that the fold considered is a flattened parallel fold. It is therefore necessary to check at least that the analysed fold belongs to class 1C. This method is useful in cases where the quality of the outcrops or the shape of the folded layers (e.g., perfect chevron folds) hamper the use of a complete Ramsay's classification.

Assuming no area change during flattening, $J = \lambda_1\lambda_2 = 1$ and $\lambda_2 = r_f$, so that the bulk shortening ε' associated with the flattening can be obtained by applying Eq. (8); then,

$$\varepsilon' = 1 - \sqrt{r_f}. \tag{26}$$

4. Bulk shortening due to buckling

Obtaining the bulk shortening ε associated with the buckling requires applying Eq. (7). This involves determining x'_0 and h from photographs of the fold, λ_1 and λ_2 from r_f ($\lambda_1 = 1/r_f$ and $\lambda_2 = r_f$ when $J = 1$), and l_0. Calculation of l_0 requires

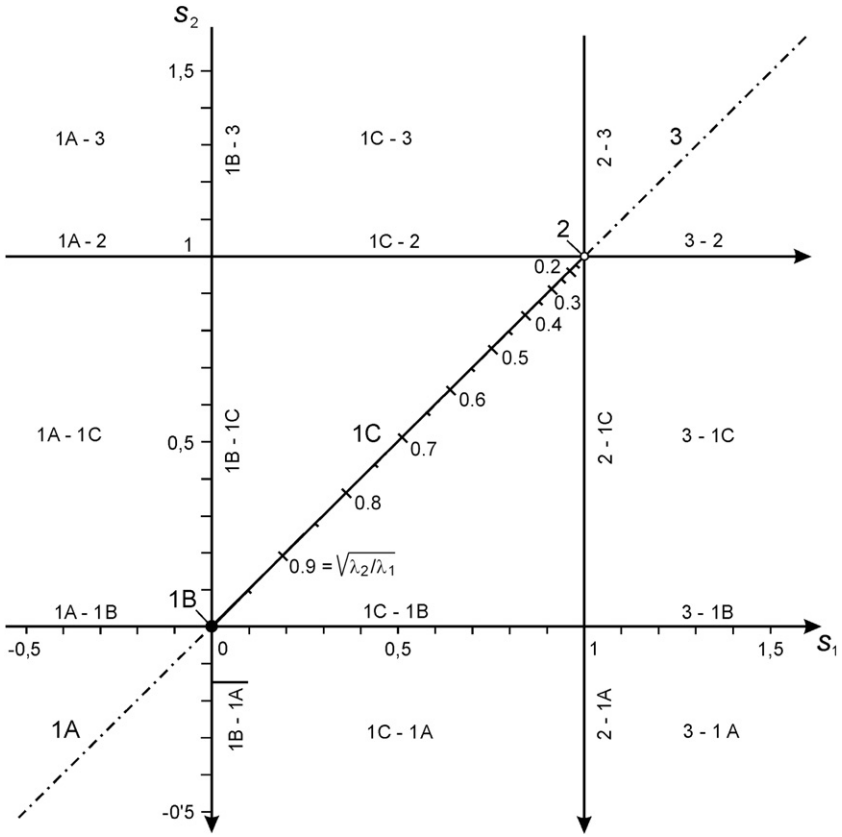

Fig. 3. Diagram of s_2 vs. s_1 showing the fold classes corresponding to the different lines and fields. The solid diagonal line is the locus of the perfect flattened parallel folds ($0 < s_1 = s_2 < 1$), and the corresponding $\sqrt{\lambda_2/\lambda_1}$ values are indicated on it.

- fitting the midline of the fold by a part of a conic section, determining the eccentricity e and the scale factor a. The equivalent methods described by Bastida et al. (1999), Aller et al. (2004), Srivastava and Lisle (2004) and Lisle et al. (2006) can be used to make this fit. The parameter a can also be determined using Eqs. (13) or (23);
- determining the parameters V, m, K and b by Eq. (15);
- applying Eq. (16) for ellipses, Eq. (17) for hyperbolas and Eq. (18) for parabolas. The calculation can be made using computer software (for example, MATHEMATICA™); and
- the data obtained in the steps above must be introduced in Eq. (7) to obtain ε.

5. Total bulk shortening

Once ε and ε' have been obtained, the total bulk shortening ε_T can be calculated using Eq. (6). When a general, rotational or irrotational, homogeneous strain is superposed on a buckle fold to produce shortening in a direction perpendicular to the axial surface, an asymmetric fold can be produced in which the bulk shortening of the two limbs is different. In this case small modifications must be made in the calculation to find separately the bulk shortening of each limb; that is, $2x_0$ and $2x'_0$ must be substituted by the width of each limb, and l_0 will have a different value for each limb. When the fold asymmetry is low, the total bulk shortening is approximately the arithmetic mean shortening of the two limbs.

A MATHEMATICA™ code to make the calculations and to automatically find the total bulk shortening is presented in Appendix A.

6. Properties of flattened parallel folds

Using the equations derived above, folds with three types of midline shape have been analysed in detail: chevron, parabolic and elliptic folds. These can be considered representative of the main shapes of folds. The results for the bulk shortening ε_T can be expressed as a function of the ratio r_f and the interlimb angle ϕ' and sets of curves of equal ϕ' (or equal h in the case of elliptic folds) for the different fold shapes analysed are shown in Fig. 4a, c and e (blue curves). These curves connect points corresponding to folds that have undergone different amounts of buckling and flattening to reach the same interlimb angle. For a specific curve, as the flattening amount increases (r_f decreases) the amplitude of the fold formed by buckling decreases. As the interlimb angle decreases a minimum in the curves appears that migrates towards higher amounts of flattening (lower values of r_f). The curves indicate that folds with the same shape and interlimb angle (or amplitude) can be formed with different amounts of bulk shortening. This is due to the fact that, starting from the same initial layer length, folds with the same shape and interlimb angle, but with different size, that is, with different length of the layer midline, can be formed. The minimum bulk shortening corresponds to the fold with the greater midline length.

As an alternative graph, sets of curves of equal ϕ' (or equal h in the case of elliptic folds) for the different fold shapes analysed are shown in Fig. 4b, d and e (blue curves), using as x-axis the thickness ratio t instead of the ratio r_f. In the case of elliptic folds, these curves coincide with those obtained with r_f as x-axis. In addition to the minimum that these curves also have, it is observed that

- for a given interlimb angle, there is a value of t beyond which total bulk strain increases explosively. This t value increases as the interlimb angle increases;
- for every interlimb angle, t has a limit value. The minimum thickness ratio for a specific interlimb angle is obtained when the flattening tends to infinity ($r_f \to 0$). In this case, the t value obtained is that of a similar fold with that interlimb angle. This value decreases with the decrease of the interlimb angle (increase of the maximum dip of the limb).
- The curves mutually cross, so that each of them crosses every other. This means that two folds with different interlimb angle can have the same thickness ratio and bulk shortening. The flattening amount involved for each of them is different, so that the fold with higher interlimb angle must have undergone more flattening than the fold with lower interlimb angle.

The red curves in Fig. 4a, c and e track the change in interlimb angle with increasing flattening, for a given value of interlimb angle after buckling. The pre-flattening condition is indicated by the intercept of the red curves with the y-axis. The blue curves and red curves thus have a common point on the y-axis that gives the value of interlimb angle after buckling and before flattening starts. The intersection points of the curves of progressive flattening (red curves) with the curves of constant interlimb angle (blue curves) track the variation of interlimb angle with the increase of flattening (e.g., points A_1, A_2, A_3 and A_4 in Fig. 4a indicate where a fold with a buckling interlimb angle of 50° is flattened to produce interlimb angles of 40, 30, 20 and 10°).

When curves of progressive flattening are plotted in the graph of ε_T against t (red and brown curves in Fig. 4b, d and e), it is observed, as in the graphics of ε_T against r_f, that they are increasing curves that have a common point on the y-axis with the blue curves of equal interlimb angle. In this case the curves corresponding to initial interlimb angle $\geq$120° cross the curves corresponding to lower initial interlimb angle and they have been drawn in brown to highlight this feature. The crossing points indicate that two folds with the same t and ε_T can be formed from buckling folds with different interlimb angle. At a crossing point, the fold originated from a buckling fold with lower interlimb angle has undergone lower flattening amount (higher r_f value) than that originating from a fold with a higher interlimb angle. The interpretation of the crossing points of the blue curves of equal ϕ' with the red and brown curves of progressive flattening is difficult, since the following types of crossing points with different meaning can be distinguished.

- Crossing points of a curve of progressive flattening with initial interlimb angle <120° (red curves in Fig. 4b and d) with the decreasing part of the curves of equal ϕ' (blue curves in Fig. 4b and d) track the variation of interlimb angle with the increase of flattening for the red curve (e.g., points B_1 and B_2 in Fig. 3b indicate where a fold with buckling interlimb angle of 30° achieves interlimb angles of 20° and 10° by flattening).
- Crossing points of a curve of progressive flattening with initial interlimb angle $\geq$120° (brown curves in Fig. 4b and d) with the subvertical part of the curves of equal ϕ' (blue curves in Fig. 4b and d) track the variation of interlimb angle with the increase of flattening for the brown curve (e.g., points C_1 to C_{12} in Fig. 4b indicate where a fold with buckling interlimb angle of 160° reaches interlimb angles of 120° to 10° by flattening).
- Crossing points of the subvertical part of a curve of equal ϕ' (blue curves in Fig. 4b and d) with a curve of progressive flattening with initial interlimb angle <120° (red curves in Fig. 4b and d) (e.g., point D in Fig. 4b), or crossing points of the decreasing part of a curve of equal ϕ' (blue curves in Fig. 4b and d) with curves of progressive flattening with initial interlimb angle $\geq$120° (brown curves in Fig. 4b and d) (e.g., point E in Fig. 4b) correspond in each case to two folds with different interlimb angle and the same values of t and ε_T.

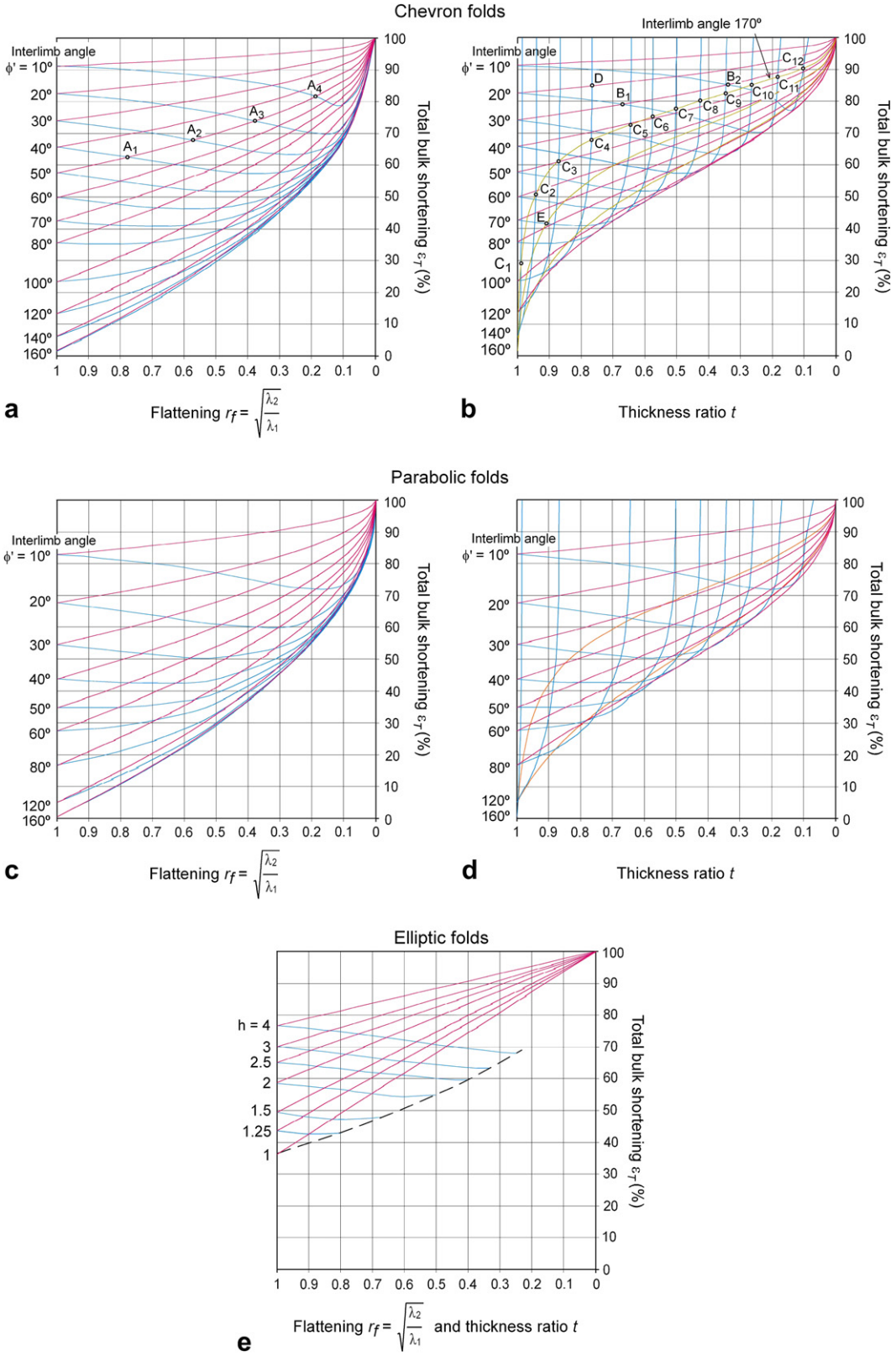

Fig. 4. Curves of total bulk shortening vs. flattening (a, c and e) and curves of total bulk shortening vs. thickness ratio (b, d and e) for three selected fold shapes. Chevron folds (a and b), parabolic folds (c and d) and elliptic folds (e). Blue lines correspond to folds with the same interlimb angle (a to d) or with the same aspect ratio (e), whereas red lines show the fold evolution during flattening for folds with the indicated initial buckling interlimb angle (a–d) or with the indicated initial aspect ratio (e). Brown lines show the fold evolution for folds with initial interlimb angles $\geq 120^{\circ}$ (a and d). See text for further explanation.

If the analysed fold has a parabolic, semielliptical or chevron shape, or one close to these, the blue curves of Fig. 4a, c and e enable an approximate estimation of the total bulk shortening ε_T from the r_f and ϕ' values of the analysed fold without calculations. Alternatively, ε_T can be also obtained from t and ϕ' values using the blue curves in Fig. 4b, d and e.

7. Example of application

The potential of the method to quantify the total bulk shortening produced in flattened parallel folds is shown by the analysis of a set of small folds developed in a multilayer of Precambrian sandstone and shale from the Narcea antiform (Westasturian-Leonese Zone, NW Spain) (Fig. 5). Forty folds developed in competent layers of sandstone were selected for the analysis. Other folds in the sample displaying complicated geometry due to accommodation problems of material, which give rise to structures such as bulbous hinges, small faults, non-plane axial surfaces, etc. were not analysed.

The first stage of the method is to obtain the strain ratio r_f due to flattening. The method based on the evaluation of parameters s_1 and s_2 has been used in this stage for most of the folds. The parameters have been obtained from measurements of orthogonal thickness and dip made on a scanned image of the sample and applying then Eqs. (24) and (25). The results are shown in Fig. 6. Most of the folds belong to class 1C, but some of the points lie too far from the line $s_1 = s_2$; the line corresponding to flattened parallel folds. A few folds belong to class 3 for high dips (corresponding to parameter s_2), that is, they are folds composed of classes 1C and 3. Only 23 class 1C folds whose plot on the diagram of s_1 vs. s_2 is located at an orthogonal distance from the line $s_1 = s_2$ of less than 0.25 have been considered as adequate for evaluating r_f. In these folds the arithmetic mean $\bar{s}$ of s_1 and s_2 for every limb has been obtained to make $\bar{s} = s_1 = s_2$. r_f Value has been obtained for every limb taking into account than $r_f = (1 - s_1)^{1/2} = (1 - s_2)^{1/2}$. The total flattening for a complete fold has been obtained by determining the arithmetic mean of r_f of the two limbs. The individual values of $\sqrt{\lambda_1}$ and $\sqrt{\lambda_2}$ can be obtained assuming no area change.

In order to quantify the bulk shortening due to buckling, we must use Eqs. (11) and (3). For that it is necessary to find a part of

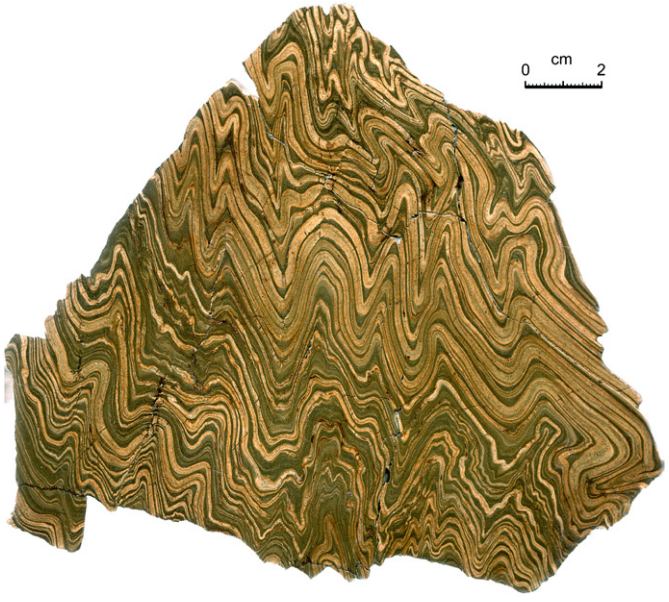

Fig. 5. Small folds in a multilayer of Precambrian sandstone and shale from the Narcea antiform (Westasturian-Leonese Zone, NW Spain).

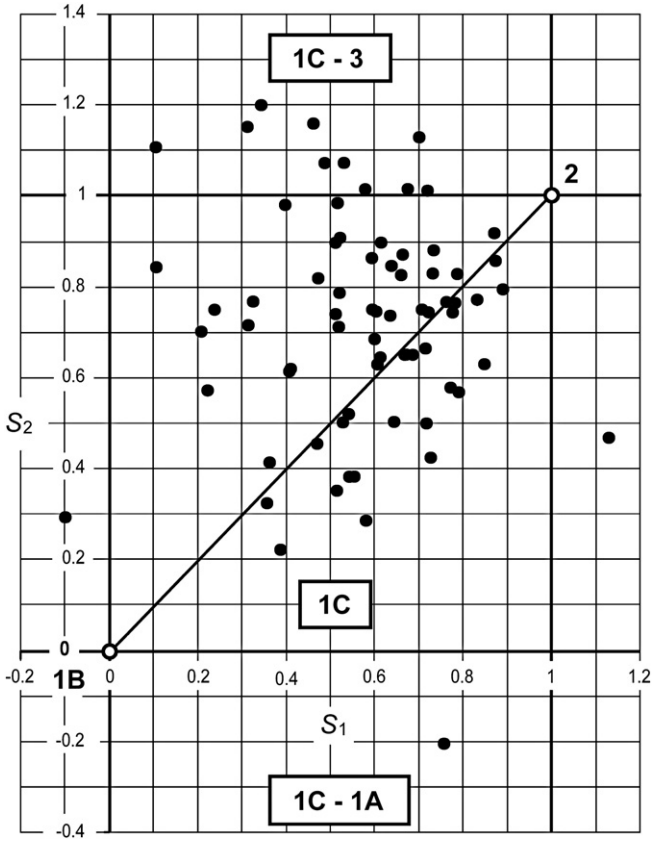

Fig. 6. Plot of selected folds from the sample in Fig. 5 on the s_1–s_2 diagram. Note the asymmetric distribution with some folds entering the 1C-3 field.

a conic section that fits the function $f(x')$ of the fold midline in the interval defined by every limb. The fit has been made firstly using the program 'Fold Profiler' described by Lisle et al. (2006) for the profile of the folded surfaces. Then, the eccentricity and aspect ratio of the midline has been approximately obtained for each limb by determining the respective arithmetic mean values of these parameters for the bottom and top of the folded layer. The arithmetic mean of the values of each of these parameters for the midline of the two limbs gives approximately the eccentricity and aspect ratio of the midline of the complete fold. The eccentricities range in general between 0.9 and 1.1 (shapes close to parabolas) and the aspect ratio is lower than 6. A simple parameter to define the function $f(x')$, an alternative to the aspect ratio, is the interlimb angle. This parameter has been measured directly form the scanned image of the sample.

Once the shortening due to buckling and flattening has been obtained, Eq. (6) can be used to determine the total bulk shortening. A MATHEMATICA™ code that automatically calculates the total bulk shortening from the $\sqrt{\lambda_1}$ due to flattening (or the thickness ratio), the eccentricity and the interlimb angle (or the aspect ratio) are shown in Appendix A. The ellipses of total bulk strain obtained for folds of the analysed sample, assuming no area change, are shown in Fig. 7. The values of total bulk shortening obtained for the folds analysed have been plotted against the interlimb angle (Fig. 8). The points are well fitted by a decreasing straight line, suggesting that the interlimb angle gives in this case a first estimation of the total bulk shortening. Nevertheless, this relation must depend also on the lithology and the deformation conditions and must be checked in other cases. The bulk shortening due to buckling and the bulk shortening due to flattening have also been plotted against the interlimb angle (Fig. 9) and the points also show a decreasing

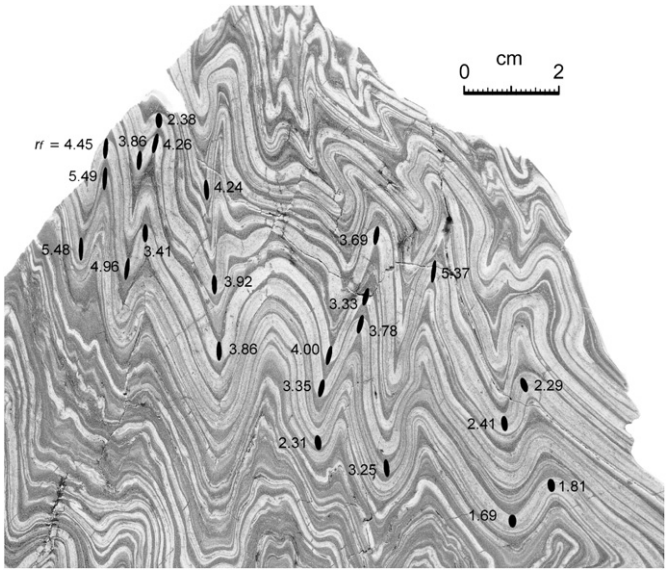

Fig. 7. Total bulk strain ellipses obtained for some of the folds in the sample of Fig. 5. The corresponding $\sqrt{\lambda_1/\lambda_2}$ values are indicated. No area change is assumed in the analysis.

tendency, though the dispersion of points is greater than in the case of the total bulk shortening, mainly in the case of flattening.

Fig. 6 also shows a tendency of points to have $s_1 < s_2$, that is, the number of points with $s_1 < s_2$ is notably greater than the number of points with $s_1 > s_2$. In addition, several points have $s_1 < 1 < s_2$, indicating that the corresponding fold limbs belong to class 3 for high dips. The formation of these latter folds in competent layers is difficult to explain. Nevertheless, several possible reasons can be pointed out to explain these facts: initial irregularities in the shape of the layers, simultaneous buckling and flattening, pressure solution and interaction between the folding layers. Now we consider briefly these factors.

Slight initial irregularities in the shape of the layer do not produce drastic deviations of the representative points from the line $s_1 = s_2$ in the diagram of s_1 vs. s_2. Assuming that the thickness of the layer is maintained during the buckling, a gentle initial taper of the layer would give rise to some differences between s_1 and s_2 after flattening, but would not systematically produce $s_1 < s_2$ and usually the whole fold would be maintained inside the field of the class 1C folds.

Simultaneous buckling and flattening is a possible mechanism that was considered by Hudeleston (1973). Usually it is admitted that flattening probably occurs when the growth of parallel folds by buckling becomes difficult (Ramsay, 1967, pp. 411–412). However, a transitional stage between buckling and flattening in which both mechanisms operate simultaneously could exist in some cases. This combination would give rise to folds with $s_1 < s_2$ (see, for example, Hudeleston, 1973, Fig. 23B), but not to folds with a part of class 3 (points with $s_1 < 1 < s_2$).

Detailed observation of folds in the analysed sample suggests that pressure solution can be an important mechanism in the development of the folded layer geometry. In many cases, relatively pale areas are observed in the dilation spaces corresponding to the hinge zones of the incompetent layers and specially near to the outer arc of the competent layers (Fig. 10). This feature suggests that quartz, which is relatively soluble by pressure solution, has been eliminated from the competent layers at the interface with the incompetent layers in the parts of the limbs with high dips, where the interface tends to be at a high angle to the main principal compressive stress. The dissolved material has probably precipitated in the dilation spaces generated during folding in the hinge zones within the incompetent layers. Where dips are high, dissolution of the competent layer could involve thinning in the limbs and lead to a switch to a class 3 fold geometry in some cases. This mechanism seems possible in small folds where the distance between inflection points and hinge zones is compatible with the short paths of the diffusion processes. Nevertheless, there is not an obvious relation between folds with evidence of pressure solution and folds with $s_1 < s_2$ or $s_1 < 1 < s_2$.

Compressive forces due to interaction between adjacent competent layers can produce local deformation in the limbs that can thin the layers and give rise to situations with $s_1 < s_2$ or even $s_1 < 1 < s_2$. These surface forces could be a cause of local pressure solution. An example can be seen at the point *P* of Fig. 10, where a competent layer penetrates slightly the adjacent competent layer, giving rise to a thinning of its limb, which classifies as 1C-3 ($s_1 < 1 < s_2$.).

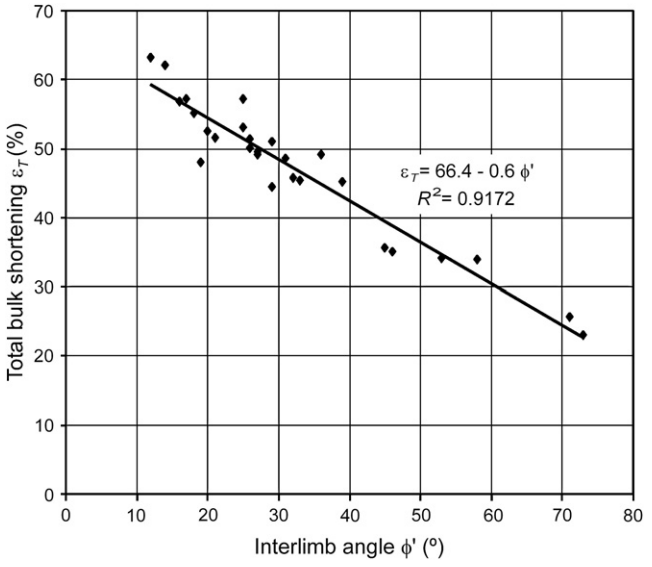

Fig. 8. Diagram of total bulk shortening vs. interlimb angle for selected folds in the sample of Fig. 5. Note the linear correlation of the values. The equation of the correlation straight line and the squared correlation R^2 value are indicated.

8. Discussion and conclusions

An analytical method to quantify the total bulk shortening in flattened parallel folds is developed in the present paper. The method requires determining first the flattening amount by any of the available methods (Ramsay, 1967; Hudeleston, 1973; Lisle, 1992, 1997; Shah and Srivastava, 2006; Srivastava and Shah, 2006), or using a new simple method proposed in the present paper. The new method is based on the use of two parameters, s_1 and s_2, that permit a simplified implementation of the Ramsay's classification scheme. In a second step, the conic section that gives the best fit to the folded layer midline is obtained using the program 'Fold Profiler' (Lisle et al., 2006). Finally the flattening and the shape data are used to compute the total bulk shortening of the folded layer. A computer code allows automating the calculations (Appendix A). Graphical determination of the bulk strain can be also made using the charts of Fig. 4.

The method proposed to quantify the total bulk strain disregards the homogeneous layer shortening that can occur at the beginning of folding, so that it only provides a minimum bulk shortening. In agreement with buckling theory (Biot, 1961; Ramberg, 1964), the amount of layer shortening decreases as the competence contrast between layers increases, so that the error will be

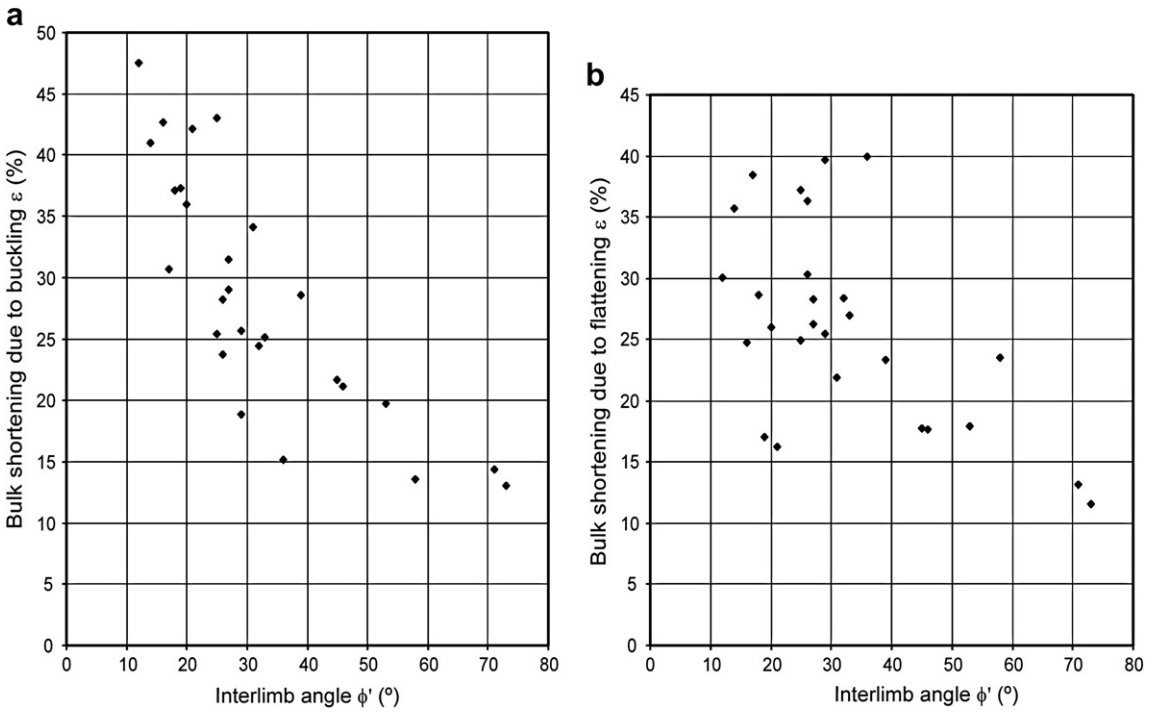

Fig. 9. Diagrams of bulk shortening due to buckling vs. interlimb angle (a) and bulk shortening due to flattening vs. interlimb angle (b) for selected folds in the sample of Fig. 5.

small with high competence contrasts. This method allows the estimation of a single total strain ellipse for each fold, and the data obtained will have a particular interest in studies of regional geology, in which an aim is to know the strain distribution in an orogenic belt.

A set of 23 small class 1C folds from a sample of sandstone and shale, collected in the Narcea antiform (Westasturian-Leonese Zone, NW Spain), was analysed in order to determine the total bulk shortening. The midlines of the folded layers have shapes close to parabolas with an aspect ratio lower than 6. The results show a near-linear negative relationship between the total bulk shortening and the interlimb angle (Fig. 8), and suggest that the interlimb angle can allow a first estimation of this shortening. Testing of this relation for folds developed in other rocks and geological conditions is an interesting topic that must be researched in the future.

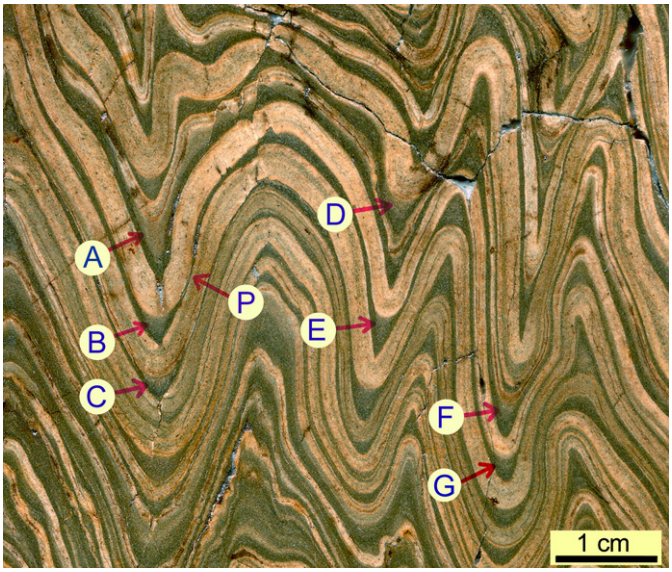

Fig. 10. Details of the Fig. 5. A–G indicate pale areas with quartz enrichment in the hinge zone of the incompetent layers that suggest a mechanism of pressure solution. *P* points to an area of interaction between adjacent competent layers that resulted in a thinning of the fold limbs.

Some of the folds of the sample above belong to class 3 or are close to it for high dips. These forms cannot be explained by homogeneous flattening of parallel folds. Folds of class 1C tending to class 3 for high dips can be explained by simultaneous buckling and flattening (Hudeleston, 1973). However, these folds, together with the class 3 folds for high dips, can be also explained by a mechanism of pressure solution that eliminates quartz from the sandstone/shale interface in the areas with high dips. Presence of pale areas enriched in quartz in the hinge zones of the incompetent layer is indicative of quartz precipitation and support this hypothesis. Interaction forces between adjacent competent layers can enhance the solution mechanism and produce an additional thinning of the limbs.

Acknowledgements

The present work was supported by Spanish CGL2005-02233-BTE project funded by Ministerio de Educación y Ciencia and Fondo Europeo de Desarrollo Regional (FEDER) and the project Topo-Iberia (CSD2006-0041) of the Spanish CONSOLIDER-INGENIO 2010 Program. We are grateful to A. Rubio Ordóñez and L.M. Rodríguez Terente for providing access to the sample analysed, and to J. R. Martínez Catalán and an anonymous reviewer for valuable suggestions that greatly improved the original manuscript.

Appendix A. MATHEMATICA code to obtain the total bulk shortening in flattened parallel folds

This appendix consists of two parts. The first contains the MATHEMATICA code where the necessary functions are defined. The second includes the most frequent applications of the previous

definitions in order to determine the bulk shortening from different inputs.

A.1. Mathematica definitions for bulk shortening analysis

The following definitions must not be modified by the user and must be run prior to all the calculations:

```
obtainLambda2[c_,v_,phi_]:=Module[{},v Sqrt[c^2-
Cos[phi Degree]^2]/Abs[Sin[phi Degree]]];

obtainLambda1[c_,v_,phi_]:=Module[{},v Abs[Sin[phi
Degree]]/Sqrt[c^2-Cos[phi Degree]^2]];

obtainAfromInterlimbAngle[xp0_,e_,phi_]:=
Module[{},xp0 Sqrt[Tan[Degree phi/2]^2+1-e^2]];

obtainAfromH[xp0_,e_,h_]:=Module
[{},xp0(1+(1-e^2)h^2)/(2 h)];

obtainMaximumDip[xp0_,e_,a_]:=Module[{},ArcTan
[(xp0/a)/Sqrt[1-(1-e^2)(xp0/a)^2]] 180/Pi];

obtainM[l1_,l2_,e_]:=Module[{},1-l1/(l2(1-
e^2))];
obtainV[xp0_,e_,a_]:=Module[{},Sqrt[Abs
[1-e^2]]xp0/a];

hMaximum[e_]:=Module[{},1/Sqrt[Abs[1-e^2]]];
integrand1[m_,t_]:=Module[{},Sqrt[(1-m    t^2)/
(1-t^2)]];

integrand2[m_,t_]:=Module[{},Sqrt[(1+m t^2)/(1+
t^2)]];

funcLongParabola[b_]:=Module[{},b Sqrt[1+b^2]+
ArcSinh[b]];

l0[l1_,l2_,xp0_,e_,a_]:=Module[{limT,m,b,coef1,-
coef2},limT=Sqrt[Abs[1-e^2]]xp0/a;m=If
[e\[Equal]1,0,obtainM[l1,l2,e]];b=Sqrt[l1/l2]
xp0/a;coef1=If[e\[Equal]1,0,2a/(Sqrt[l1]
Sqrt[Abs[1-e^2]])];coef2=a Sqrt[l2]/l1;
Which[
  e<1,coef1 NIntegrate[integrand1[m,t],
  {t,0,limT}],
  e>1,coef1 NIntegrate[integrand2[m,t],
  {t,0,limT}],
  e\[Equal]1,coef2 funcLongParabola[b]]];

shorteningBuckleFold[l1_,l2_,xp0_,e_,a_]:
=1-2xp0/(Sqrt[l1]l0[l1,l2,xp0,e,a]);

shorteningFlattenedFold[l1_,l2_,xp0_,e_,a_]:
=1-Sqrt[l1];

totalShortening[l1_,l2_,xp0_,e_,a_]:=1-2xp0/
l0[l1,l2,xp0,e,a];
```

A.2. Examples of application of the code for the determination of the bulk shortening.

In this part the total bulk shortening is determined from different sets of data inputs. The cases are presented with particular inputs that can be modified by the user. In the following text, the names of the functions defined above are in bold and the variables defined by the user are in italics.

Case 1: Obtaining the bulk shortening from the interlimb angle *phi* and the thickness ratio *c*.

Data input: Area change, interlimb angle *phi*, final width of the fold limb *xp0* (usually considered unity), eccentricity of the conic section *e* and thickness ratio *c*.

```
areaChange=1;
phi=37;
xp0=1;
e=1.04095;
c=0.551162;
```

Obtaining the scale factor *a* of the conic section (input and output data are displayed on the same line separated by an arrow):

```
a=obtainAfromInterlimbAngle[xp0,e,phi] →
0.168455
```

Obtaining the maximum dip:

```
maximumDip=obtainMaximumDip[xp0,e,a] → 71.5
```

Obtaining the principal values of the strain:

```
lambda2=obtainLambda2[c,areaChange,
maximumDip] → 0.475221
lambda1=obtainLambda1[c,areaChange,
maximumDip] → 2.10428
```

Obtaining the shortening due to buckling:

```
shorteningBuckleFold[lambda2,lambda1,xp0,e,a] →
0.292994
```

Obtaining the shortening due to flattening:

```
shorteningFlattenedFold[lambda2,lambda1,
xp0,e,a] → 0.310637
```

Obtaining the total bulk shortening:

```
totalShortening[lambda2,lambda1,xp0,e,a] →
0.512616
```

Case 2: Obtaining the bulk shortening from the aspect ratio *h* and the thickness ratio *c*.

Data input: Area change, aspect ratio *h*, final width of the fold limb *xp0* (usually considered unity), eccentricity of the conic section *e* and thickness ratio *c*.

```
areaChange=1;
h=2;
xp0=1;
e=0.999999;
c=0.7;
```

Obtaining the maximum possible *h* for the eccentricity *e* (*h* value in the inputs must be lower than *h* maximum for the problem to be solvable):

```
hMaximum[e] → 707.107
```

Obtaining the scale factor *a* corresponding to the aspect ratio *h*:

```
a=obtainAfromH[xp0,e,h] → 0.250002
```

Obtaining the maximum dip:

```
maximumDip=obtainMaximumDip[xp0,e,a] → 75.9639
```

Obtaining the principal values of the strain:

```
lambda2 = obtainLambda2[c, areaChange, maximumDip] →
0.67685
lambda1 = obtainLambda1[c, areaChange,
maximumDip] → 1.47743
```

Obtaining the shortening due to buckling:

```
shorteningBuckleFold[lambda2, lambda1, xp0, e, a] →
0.432152
```

Obtaining the shortening due to flattening:

```
shorteningFlattenedFold[lambda2, lambda1,
xp0, e, a] → 0.177291
```

Obtaining the total bulk shortening:

```
totalShortening[lambda2, lambda1, xp0, e, a] →
0.532827
```

Case 3: Obtaining the bulk shortening from the inte rlimb angle *phi* and the principal values of strain *lambda2* and *lambda1*.

Data input: interlimb angle *phi*, final width of the fold limb *xp0* (usually considered unity), eccentricity of the conic section *e*, *lambda1* and *lambda2*.

```
phi = 36;
xp0 = 1;
e = 0.9;
lambda2 = 0.03216996;
lambda1 = 1/0.03216996;
```

Obtaining the maximum possible *h* for the eccentricity *e* (*h* value in the inputs must be lower than *h* maximum for the problem to be solvable):

```
hMaximum[e] → 2.29416
```

Obtaining the scale factor *a* of the conic section from the interlimb angle *phi*:

```
a = obtainAfromInterlimbAngle[xp0, e, phi] →
0.543666
```

Obtain the maximum dip:

```
maximumDip = obtainMaximumDip[xp0, e, a] → 72
```

Obtaining the shortening due to buckling:

```
shorteningBuckleFold[lambda2, lambda1, xp0, e, a] →
0.0298474
```

Obtaining the shortening due to flattening:

```
shorteningFlattenedFold[lambda2, lambda1,
xp0, e, a] → 0.576491
```

Obtaining the total bulk shortening:

```
totalShortening[lambda2, lambda1, xp0, e, a] →
0.589132
```

Case 4: Obtaining the bulk shortening from the aspect ratio *h* and the principal values of strain *lambda1* and *lambda2*.

Data input: interlimb angle *phi*, final width of the fold limb *xp0* (usually considered unity), eccentricity of the conic section *e*, *lambda1* and *lambda2*.

```
h = 2;
xp0 = 1;
e = 0.999999;
lambda2 = 0.64;
lambda1 = 1/lambda2;
```

Obtaining the maximum possible *h* for the eccentricity *e* (*h* value in the inputs must be lower than *h* maximum for the problem to be solvable):

```
hMaximum[e] → 707.107
```

Obtaining the scale factor of the conic section *a* corresponding to the aspect ratio *h*:

```
a = obtainAfromH[xp0, e, h] → 0.250002
```

Obtaining the maximum dip:

```
maximumDip = obtainMaximumDip[xp0, e, a] → 75.9639
```

Obtaining the shortening due to buckling:

```
shorteningBuckleFold[lambda2, lambda1, xp0, e, a] →
0.411842
```

Obtaining the shortening due to flattening:

```
shorteningFlattenedFold[lambda2, lambda1, xp0,
e, a] → 0.2
```

Obtaining the total bulk shortening:

```
totalShortening[lambda2, lambda1, xp0, e, a] →
0.529474
```

References

Abramowitz, M., Stegun, I.A., 1964. Handbook of mathematical functions with formulas, graphs and mathematical tables. In: National Bureau of Standards, Applied Mathematics Series 55. National Bureau of Standards, Washington, 1046 pp.

Aller, J., Bastida, F., Toimil, N.C., Bobillo-Ares, N.C., 2004. The use of conic sections for the geometrical analysis of folded surface profiles. Tectonophysics 379, 239–254.

Bastida, F., Aller, J., Bobillo-Ares, N.C., 1999. Geometrical analysis of folded surfaces using simple functions. Journal of Structural Geology 21, 729–742.

Bastida, F., Bobillo-Ares, N.C., Aller, J., Toimil, N.C., 2003. Analysis of folding by superposition of strain patterns. Journal of Structural Geology 25, 1121–1139.

Bastida, F., Aller, J., Bobillo-Ares, N.C., Toimil, N.C., 2005. Fold geometry: a basis for their kinematical analysis. Earth-Science Reviews 70, 129–164.

Biot, M.A., 1961. Theory of folding of stratified visco-elastic media and its implications in tectonics and orogenesis. Geological Society of America Bulletin 75, 563–568.

Bobillo-Ares, N.C., Bastida, F., Aller, J., 2000. On tangential longitudinal strain folding. Tectonophysics 319, 53–68.

Bobillo-Ares, N.C., Toimil, N.C., Aller, J., Bastida, F., 2004. FoldModeler": a tool for the geometrical and kinematical analysis of folds. Computers and Geosciences 30, 147–159.

Bobillo-Ares, N.C., Aller, J., Bastida, F., Lisle, R.J., Toimil, N.C., 2006. The problem of area change in tangential longitudinal strain folding. Journal of Structural Geology 28, 1835–1848.

Hudeleston, P.J., 1973. Fold morphology and some geometrical implications of theories of fold development. Tectonophysics 16, 1–46.

Hudleston, P.J., Lan, L., 1993. Information from fold shapes. Journal of Structural Geology 15, 253–264.

Lisle, R.J., 1992. Strain estimation from flattened buckle folds. Journal of Structural Geology 14, 369–371.

Lisle, R.J., 1997. A fold classification scheme based on a polar plot of inverse layer thickness. In: Sengupta, S. (Ed.), Evolution of Geological Structures in Micro- to Macro-scales. Chapman and Hall, pp. 323–339.

Lisle, R.J., Fernández Martínez, J.L., Bobillo-Ares, N.C., Menéndez, O., Aller, J., Bastida, F., 2006. FOLD PROFILER: A MATLAB®-based program for fold shape classification. Computers and Geosciences 32, 102–108.

Mukhopadhyay, D., 1965. Effects of compression on concentric folds and mechanism of similar folding. Journal of the Geological Society of India 6, 27–41.

Ramberg, H., 1964. Selective buckling of composite layers with contrasted rheological properties. Tectonophysics 1, 307–341.

Ramsay, J.G., 1962. The geometry and mechanics of formation of "similar" type folds. Journal of Geology 70, 309–327.

Ramsay, J.G., 1967. Folding and Fracturing of Rocks. Mc-Graw Hill Book Company, New York, 568 pp.

Shah, J., Srivastava, D.C., 2006. Strain estimation from flattened parallel folds: application of the Wellman method and Mohr circle. Geological Magazine 143, 243–247.

Srivastava, D.C., Lisle, R.J., 2004. Rapid analysis of fold shape using Bézier curves. Journal of Structural Geology 26, 1553–1559.

Srivastava, D.C., Shah, J., 2006. A rapid method for strain estimation from flattened parallel folds. Journal of Structural Geology 28, 1–8.